Hindawi
International Journal of Energy Research
Volume 2024, Article ID 5543500, 21 pages
https://doi.org/10.1155/2024/5543500

Research Article

Probabilistic Energy Management of DGs and Electric Vehicle Parking Lots in a Smart Grid considering Demand Response

Ebrahim Razaghi Ghadikolaei, Alireza Ghafouri, and Mohsen Sedighi

Department of Electrical Engineering, Sari Branch, Islamic Azad University, Sari, Iran

Correspondence should be addressed to Alireza Ghafouri; ghafouri@iausari.ac.ir

Received 28 July 2023; Revised 21 September 2023; Accepted 1 February 2024; Published 22 February 2024

Academic Editor: Longxing Wu

In this paper, a novel model of an energy management system (EMS) for a microgrid (MG) under uncertain conditions is proposed. The MG consists of renewable photovoltaic and wind sources along with electric vehicle parking lots. Hence, the model incorporates the uncertainties of renewable DGs, parking lots, and also load. In this study, the MG operation cost and voltage stability index are considered objective functions. A novel combined algorithm (hMOPSO-HS) is proposed for microgrid energy management. The hMOPSO-HS algorithm is a combination of the mutant multiobjective particle swarm optimization (MOPSO) algorithm and the harmony search (HS) algorithm. The simulations are performed in two parts, with and without considering the uncertainty. The comparative analysis involves evaluating the optimization outcomes achieved by the hMOPSO-HS algorithm in contrast to various other metaheuristic algorithms for multiobjective optimization. The simulation findings validate the superior efficacy of the hMOPSO-HS algorithm compared to other approaches. Also, the simulation results showed that in the conditions of uncertainty, the operating cost is 6.1% higher and the microgrid stability index is 6.8% lower. Also, considering the uncertainty has caused the penalty for energy not supplied (ENS) and demand response program (DRP) costs to increase by 3% and 4%, respectively.

1. Introduction

Energy management in microgrids (MGs) is a crucial aspect of power system studies. It encompasses various objectives, including cost reduction, emission reduction, enhanced reliability, and improved power quality. A microgrid typically comprises key components such as power sources, electrical storage, and loads. The DGs in a microgrid can be renewable, such as photovoltaic (PV) arrays and wind turbines (WTs), or nonrenewable sources as well as microturbines. Additionally, electrical energy storage can be achieved through battery storage banks or electric vehicle (EV) parking lots (PLs). Smart parking lots integrated into the microgrid provide various functionalities, including improvements in system power quality and also reliability, maintaining voltage stability, minimizing losses, and increasing profitability for EV owners [1]. Maximizing profitability and enhancing reliability are crucial aspects of smart parking utilities, particularly in their significance. To achieve these objectives, a comprehensive scheduling approach is required for EV charging and discharging programming. In recent years, a plethora of research investigations has been carried out in the domain of EMS, delving into diverse concepts and methodologies [2].

In [3], a novel approach is presented for coordinating the EV charging in the MG. The method aims to improve MG reliability by minimizing the charging costs of EVs. To achieve this, it considered the electric energy price uncertainty in the market and the charging time of EVs. In [4], a daily energy management model is introduced to enhance MG reliability in the context of a substantial number of electric vehicles (EVs) being present. The model allows vehicle owners to manage energy consumption during their travels through effective energy management techniques. In [5], a simulation technique utilizing probabilistic indices is employed to enhance the reliability of MGs with DG sources and EVs, particularly in island mode. In [6], an efficient objective function is put forth to diminish the operational

costs of an MG with a significant number of EVs and DGs. In [7], the study focuses on the calculation details of MG reliability that incorporates both DG sources and EVs. [8] presents an economic-based optimization approach for EVs in the MG, specifically considering cogeneration, while also taking into account MG reliability indexes as operational constraints. In [9], the energy not supplied criterion (ENS) and the time of MG connection to the network are utilized to evaluate MG reliability. [10] investigates both economic and reliability aspects of the MG, using real-time pricing for power exchange transactions of the MG and parking lots (PLs) and employing a probabilistic method to calculate network reliability with and without DG sources and EVs. [11] proposes an energy management system for EV charging in the power system through a DRP, aiming to reduce operation costs and enhance MG reliability, with customer participation encouraged for effective energy management. [12] employs a DRP to improve distribution network characteristics, leveraging EV charging stations to enhance network reliability, with simulation results showing a significant reduction in ENS value through load response programs and scheduled EV charging. [13] introduces an intelligent algorithm based on neural networks for the microgrid EMS, highlighting the impact of DR on MG power exchange and EV charging/discharging. [14] proposes an optimal EMS approach for a MG incorporating PV panels, EVs, and responsive loads, considering load uncertainty and indicating a cost reduction of about 2.5% with the use of DR programs. [15] focuses on MG energy management with peak load management, aiming to reduce operating costs using time of use (TOU) pricing, incorporating an error function to calculate uncertainty in different scenarios. [16] defines demand response programs (DRPs) as changes in electricity consumption patterns in response to time-varying prices, including incentive payments to reduce consumption during high-price or reliability issue periods. [17] explores DRPs through pricing methods that incentivize consumers to shift their electricity demand away from peak times, highlighting the advantage of avoiding expensive peak-time power plant construction. In [18], a demand DRP is introduced for grid-connected EVs. The primary aim of this study is to conduct a comparative analysis of different approaches for managing EVs in the day-ahead scenario.

In [19], the study addresses the optimal scheduling of electric vehicle (EV) charge and discharge, taking into account uncertainty in electricity prices. The objective function is designed to maximize network profitability. [20] focuses on microgrid (MG) energy management with EVs and DG sources, aiming to improve MG reliability indices while considering uncertainties associated with DGs. [21] presents an optimal EV charge and discharge strategy considering uncertainties in EV and DG operations, with the objective function aimed at cost reduction and pollution mitigation based on probabilistic behaviors of EV and wind turbine charging and discharging. [22] introduces a scheduling method for optimizing the utilization of MG infrastructure during nonpeak times for EV charging, considering environmental and economic factors to effectively integrate a significant number of electric vehicles (EVs) into the network accounting for their uncertainties. In [23], a novel approach to microgrid EMS is proposed, considering the presence of electric vehicles (EVs), aiming to achieve maximum profitability in the standard 33-bus power system by reducing generation costs considering uncertainties in energy market prices and EV charging times. In [24], an energy management system is proposed that takes into account the uncertainties associated with electric vehicles and wind turbines.

This paper explores the influence of uncertainties on both EMS and system reliability. A stochastic energy management approach is employed for an MG featuring smart parking lots and photovoltaic and wind energy sources, with the aim of reducing operational costs and enhancing reliability. Additionally, a novel cost-based objective function is introduced, taking into account the probability of different scenarios occurring. Finally, a novel and innovative combined algorithm is put forward to address the optimization challenge. The proposed algorithm is a combination of the mutant MOPSO and HS algorithms. Therefore, the main contributions to this paper are as follows:

(i) Assess the probabilistic EMS of EV parking lots and renewable DGs with the objectives of cost reduction and enhancement of system voltage stability

(ii) A novel weighted objective function is introduced, which takes into account the probability of scenario occurrence

(iii) A new innovative hybrid multiobjective algorithm with high accuracy is proposed

2. Problem Formulations

For an MG study, there is an essential need to provide a suitable model of the MG to consider the uncertainties. Various goals such as cost reduction, improved voltage stability index, reliability, and power quality are desired and are considered for MG energy management. Ensuring the provision of electrical energy at the lowest cost while minimizing the occurrence of blackouts is of utmost importance [25]. In the subsequent sections, we present the formulation of objective functions for the EMS problem in a MG under uncertain conditions.

2.1. Proposed Objective Functions. The initial objective function pertains to the MG cost with the PL.

The proposed MG operation cost is a combination of the energy purchasing cost from the power system, DG power cost, EV parking cost, penalty cost for energy not supplied (ENS), and DRP cost. The first objective function can be formulated as follows:

$$F_1 = \sum_{h=1}^{Nh} \pi_h \sum_{t=1}^{T} \text{cost}(t,h) = \min \sum_{s=1}^{N_K} \pi_\kappa \sum_{t=1}^{T} \left(C_{t,h}^{\text{grid}} + \sum_{i=1}^{N_{\text{DG}}} C_{t,h,i}^{\text{DG}} + \sum_{j=1}^{N_{\text{PL}}} C_{t,h,j}^{\text{PL}} + C_{t,h}^{\text{ENS}} + C_{t,h}^{\text{DR}} \right), \tag{1}$$

where $C_{t,h}^{\text{grid}}$, $C_{t,h,i}^{\text{DG}}$, $C_{t,h,j}^{\text{PL}}$, $C_{t,h}^{\text{ENS}}$, and $C_{t,h}^{\text{DR}}$ represent the costs associated with purchasing energy from the power system, DGs, electric vehicle parking lots, energy not supplied (ENS) penalties, and DRP costs at time t, respectively. Also, π_h represents the selected scenario probability, Nh denotes the number of samples, N_{PL} signifies the number of PLs, and N_{DG} indicates the number of distributed generators. Finally, T is a period which is 24 hours. Also, in this paper, the time interval is considered one hour. The energy procurement cost from the power system is expressed as follows [26]:

$$C_{t,h}^{\text{grid}} = P_{t,h}^{\text{grid}} \times B_t^{\text{grid}}, \tag{2}$$

where $P_{t,h}^{\text{grid}}$ represents the quantity of exchanged electric power with the upstream power network and B_t^{grid} denotes the market energy price. The operation cost of the distributed generator is computed according to the following equation [27]:

$$C_{t,h,i}^{\text{DG}} = \alpha \times \left(P_{t,h,i}^{\text{DG}}\right)^2 + \beta \times P_{t,h,i}^{\text{DG}} + \gamma, \tag{3}$$

where $P_{t,h,i}^{\text{DG}}$ represents the power generated by the i^{th} distributed generator at the h-level demand. Furthermore, α, β, and γ are specific cost values associated with each unit. The cost of the PL is determined using the following equation:

$$C_{t,h,j}^{\text{PL}} = P_{t,h,j}^{\text{charge}} \times B_j^{\text{charge}} + P_{t,h,j}^{\text{discharge}} \times B_j^{\text{discharge}}, \tag{4}$$

where $P_{t,h,j}^{\text{charge}}$ and $P_{t,h,j}^{\text{discharge}}$ represent the quantities of power used for charge and discharge in the j^{th} parking lot. B_j^{charge} and $B_{t,h,j}^{\text{discharge}}$ denote the electricity prices for EV charge and discharge in the parking lot [28]. The ENS penalty is determined using the following equation:

$$C_{t,h}^{\text{ENS}} = \left(P_{t,h}^{\text{LPSP}} + P_{t,h}^{\text{UW}}\right) \times R_{t,h}^{\text{ENS}}, \tag{5}$$

where $P_{t,h}^{\text{LPSP}}$ and $P_{t,h}^{\text{UW}}$ represent the power shortage probability and the penalty for undesired power deficit. It is assumed that $P_{t,h}^{\text{UW}}$ accounts for 1% of the total load in the microgrid. The cost of the DRP is determined using the following equation:

$$C_{t,h}^{\text{DR}} = P_{t,h}^{\text{DR}} \times R_{t,h}^{\text{DR}}, \tag{6}$$

where $P_{t,h}^{\text{DR}}$ represents the reduction in power consumption by user participating in the demand response program, while $R_{t,h}^{\text{DR}}$ signifies the compensation provided to them for their reduced consumption [29].

The voltage stability index (VSI) of the power system is regarded as an additional optimization objective. Equation (7) is employed to calculate the VSI.

$$F_2 = \frac{1}{\text{VSI}(n_i)} = \frac{1}{|V_{mi}|^4 - 4[P_{ni}(ni)R_{ni} + Q_{ni}(ni)X_{ni}]|V_{mi}|^2 - 4[P_{ni}(ni)R_{ni} + Q_{ni}(ni)X_{ni}]^2}, \tag{7}$$

where P_n and Q_n are the load active power and load reactive power, respectively, V_m represents the m^{th} bus voltage, and Rn and Xn are the resistance and line impedance between the bus n and m. Figure 1 shows part of a radial distribution feeder.

2.2. Constraints

2.2.1. Generation and Load Balance Constraint. The initial restriction focuses on ensuring an equilibrium between power generation and load within the microgrid as

$$P_{t,h}^{\text{grid}} + P_{t,h}^{\text{PV}} + P_{t,h}^{\text{WT}} + P_{t,h}^{\text{discharge}} = P_{t,h}^{\text{Load}} - P_{t,h}^{\text{defict}} - P_{t,h}^{\text{UW}} + P_{t,h}^{\text{loss}} + P_{t,h}^{\text{charge}}, \forall t \in \{1, \cdots, T\}, \tag{8}$$

where $P_{t,h}^{\text{PV}}$ and $P_{t,h}^{\text{WT}}$ are the photovoltaic and wind turbine generation capacity, respectively. $P_{t,h}^{\text{defict}}$ and $P_{t,h}^{\text{Load}}$ are the amount of the nonsupplied power and power consumption.

2.2.2. DG Constraints. Two additional constraints relate to the maximum and minimum production capacities of the distributed generators. These limitations are expressed by

$$P^{\text{DG-min}} \times u(t) \le P_{t,h,}^{\text{DG}} \le P^{\text{DG-max}} \times u(t), \forall t \in \{1, \cdots, T\}, \tag{9}$$

where $P^{\text{DG-max}}$ and $P^{\text{DG-min}}$ are DG generation capacity. The binary variable $u(t)$ indicates the status of the DG units (i.e., whether they are offline or online).

2.2.3. Power System Constraint. The transfer of electrical power between the microgrid and the power system is constrained by the following:

$$P_{t,h}^{\text{grid}} \le P^{\text{grid-max}}, \tag{10}$$

where $P_{t,h}^{\text{grid}}$ represents the amount of energy exchanged with the power system and $P^{\text{grid-max}}$ denotes the upper limit on the power capacity that can be transferred to/from the upstream power network.

2.2.4. Parking Lot Constraints. For each planning time, it is not possible for the charging and discharging of electric

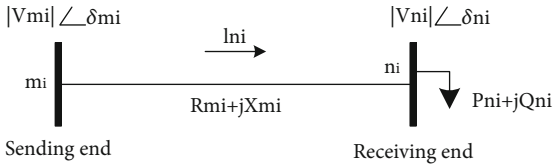

Figure 1: Section of the radial branch in the distribution network.

vehicle batteries to occur simultaneously, as indicated in the following equation:

$$A_{t,n} + B_{t,n} \leq 1, A, B \in \{0, 1\}, \forall n \in \{1, \cdots, N_{EV}\}, \forall t \in \{1, \cdots, T\}, \tag{11}$$

where $A_{t,n}$ and B_{t-n} are the binary indicating the EVs charge and discharge of the n^{th} electric vehicle PL. The constraints on the charge and discharge ratios of each EV are defined by the following limitations [30]:

$$\begin{aligned} P_{t,h,n}^{\text{EV-charge}} &\leq \left(P_n^{\text{charge-max}} \times A_{t,n}\right), \forall n \in \{1, \cdots, N_{EV}\}, \forall t \in \{1, \cdots, T\}, \\ P_{t,h,n}^{\text{EV-discharge}} &\leq \left(P_n^{\text{discharge-max}} \times B_{t,n}\right), \forall n \in \{1, \cdots, N_{EV}\}, \forall t \in \{1, \cdots, T\}. \end{aligned} \tag{12}$$

In equations (13) and (14), Ω and Ψ denote the maximum charging and discharging rates of the n^{th} electric vehicle (EV) battery, respectively. The energy stored in the EV batteries must satisfy predetermined lower and upper limits, as expressed in equations (13) and (14).

$P_n^{\text{charge-max}}$ and $P_n^{\text{discharge-max}}$ represent the charging and discharging rates of the electric vehicle. The energy stored in the batteries must comply with the predetermined minimum band and maximum band, as outlined in the following equations:

$$E_{t,h,n}^{S} \leq \psi_n^{\text{charge-max}}, \forall n \in \{1, \cdots, N_{EV}\}, \forall t \in \{1, \cdots, T\}, \tag{13}$$

$$E_{t,h,n}^{S} \geq \psi_n^{\text{charge-min}}, \forall n \in \{1, \cdots, N_{EV}\}, \forall t \in \{1, \cdots, T\}, \tag{14}$$

where $E_{t,h,n}^{S}$ is the charging mode of the EV, $\psi_n^{\text{charge-max}}$ and $\psi_n^{\text{charge-min}}$ are the battery state of charge (SOC) and depth of discharge (DOD). These limitations are implemented to safeguard against battery degradation and extend battery lifespan. $E_{t,h,n}^{S}$ is calculated by

$$E_{t,h,n}^{S} = E_{(t-1),h,n}^{S} + \eta_n^{\text{charge}} \times P_{t,h,n}^{\text{EV-charge}} - E_{t,h,n}^{\text{trip}} - \frac{1}{\eta_n^{\text{discharge}}} \times P_{t,h,n}^{\text{EV-discharge}}, \tag{15}$$

where $E_{(t-1),h,n}^{S}$ represents the residual energy from the previous time interval, $E_{t,h,n}^{\text{trip}}$ is traveling energy consumption, $P_{t,h,n}^{\text{EV-charge}}$ and $P_{t,h,n}^{\text{EV-discharge}}$ are the discharge and charge power of n^{th} electric vehicle in period t, η_n^{charge} represents charging efficiency, and $\eta_n^{\text{discharge}}$ represents discharging efficiency.

3. Uncertainty Modeling

3.1. The Proposed Model Incorporates Uncertainties. Given the increasing trend of MG privatization and the dynamic nature of load and production, managing uncertainties is crucial for ensuring the power system's reliability, operation, and control. The MG uncertainty emerges due to the absence of accurate data on the MG parameters. The primary sources of the MG uncertainty include variations in parameters over time, unanticipated dynamics, and measurement errors.

3.1.1. Electrical Demand Uncertainty. Electrical demand, being the primary source of uncertainty, significantly influences the performance of microgrids (MGs). Demand changes in MGs are primarily influenced by two factors: time and weather. The daily and weekly variations in demand are largely driven by the energy usage patterns of the user. The load changes are suitably characterized by a normal probability density function (PDF) as

$$f\left(P^{\text{Load}}\right) = \frac{1}{\sigma^{P^{\text{Load}}} \times \sqrt{2\pi}} \exp\left(-\frac{\left(P^{\text{Load}} - \mu^{P^{\text{Load}}}\right)^2}{2 \times \left(\sigma^{P^{\text{Load}}}\right)^2}\right), \tag{16}$$

where P^{Load} is the electrical demand, $\mu^{P^{\text{Load}}}$ is the demand mean, and $\sigma^{P^{\text{Load}}}$ is the demand variance [31].

3.1.2. Irradiation Uncertainty. The generation capacity of each photovoltaic array is influenced by deterministic factors such as solar radiation, panel surface temperature, panel surface area, and efficiency. Nevertheless, owing to the stochastic nature of solar irradiation, the power output of a photovoltaic array is subject to probabilistic variations. The behavior of PV units is described using the beta PDF, as shown in the following equation [32]:

$$f_{t,h}^{\text{pv}}(\text{si}_{t,h}) = \begin{cases} \dfrac{\Gamma(\alpha+\beta)}{\Gamma(\alpha).\Gamma(\beta)} (si_{t,h})^{\alpha-1} (1 - si_{t,h})^{\beta-1} & \text{for } \alpha > 0, \beta > 0, \\ 0 & \text{otherwise,} \end{cases} \tag{17}$$

where $si_{t,h}$ (kW/m^2) is solar radiation intensity, Γ is the gamma function, and also α and β represent the parameter

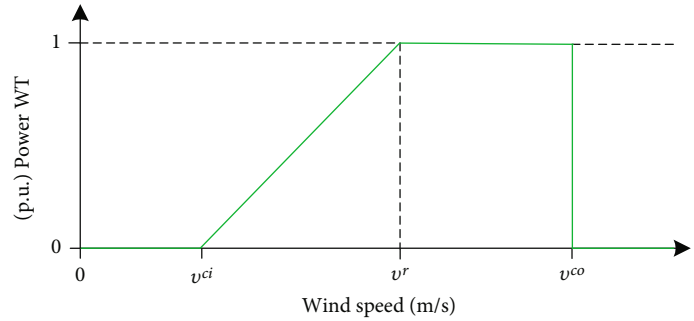

Figure 2: Power curve of a typical WT.

of beta PDF. These parameters can be calculated by the following equations:

$$\beta = \left(1-\mu^S\right)\left(\frac{\mu^S\left(1-\mu^S\right)}{\left(\sigma^S\right)}-1\right),$$
$$\alpha = \frac{\mu^S\beta}{1-\mu^S}. \tag{18}$$

Equation (19) is used to calculate the power generated by PV units in each hour.

$$P^{\mathrm{pv}}\left(\mathrm{si}_{t,h}\right) = \eta^{\mathrm{pv}} \times A^{\mathrm{pv}} \times \mathrm{si}_{t,h}, \tag{19}$$

where η^{pv} represents the PV system efficiency and A^{pv} (m^2) represents the photovoltaic surface area. The generation capacity of the photovoltaic system is formulated as

$$P_{t,h}^{\mathrm{PV}} = P^{\mathrm{PV,rated}} \times f^{PV} \times \left[\frac{G_{t,h}}{G^{\mathrm{STC}}} + \lambda^T\left(\mathrm{T}_{t,h} - T^{\mathrm{STC}}\right)\right], \tag{20}$$

where $P^{\mathrm{PV,rated}}$ is the photovoltaic array nominal capacity, f^{PV} is dirtiness factor, $G_{t,h}$ and G^{STC} are the real-time irradiation and the array standard irradiation, λ^T is temperature parameter, and $T_{t,h}$ and T^{STC} are the array real-time temperature and its standard temperature. It is worth mentioning that G^{STC} and T^{STC} are 1000 w/m^2 and 25°C [32].

3.1.3. Wind Turbine Model. In this paper, a variable-speed turbine is utilized, and its generation power is directly influenced by the uncertainty in wind velocity [33]. The stochastic nature of wind velocity can be described by utilizing the Weibull PDF, as depicted in the following equation:

$$f_{t,h}^{\mathrm{WT}}(v) = \begin{cases} \dfrac{k}{\Omega} \times \left(\dfrac{v_{t,h}}{\Omega}\right)^{K-1} \exp\left(-\left(\dfrac{v_{t,h}}{\Omega}\right)^{K}\right), & \text{for } \Omega > 1, k > 0, \\ 0 & \text{otherwise,} \end{cases} \tag{21}$$

Table 1: Parameters of the probability density functions for arrival and departure.

Arrival	K	Ω
	18.91	5.90
Departure	μ	σ
	2.21	0.30

where $f_{t,h}^{\mathrm{WT}}(v)$ is the Weibull PDF, $v_{t,h}$(m/s) is the wind speed, and k and Ω represent the shaping parameter and scaling parameter, respectively, which can be calculated using the following equations:

$$K = \left(\frac{\sigma^v}{\mu^v}\right)^{-1.088},$$
$$\Omega = \frac{\mu^v}{\Gamma\left(1+1/k\right)}, \tag{22}$$

where μ^v is the mean of wind speed data and σ^v is the wind speed data variance. The power generation capability of the WT can be determined by utilizing the following equation:

$$P^{\mathrm{WT}}(v) = \begin{cases} 0 & v \le v^{ci} \text{ or } v \ge v^{co}, \\ P^r\left(\dfrac{v - v^{co}}{v^r - v^{co}}\right) & v^{ci} < v < v^r, \\ P^r & v^r < v < v^{co}, \end{cases} \tag{23}$$

where $P_{t,h}^{\mathrm{WT}}$ is the generated turbine power and P^r is the WT nominal capacity. Also, $v^{\text{cut-in}}$ is the cut-in velocity, $v^{\text{cut-out}}$ is the cut-off velocity, and v^r is the rated velocity of a WT, respectively. The power generation curve as a function of wind speed variations is depicted in Figure 2.

3.1.4. The PL Uncertainties. The characterization of the input/output power of parking lots relies on multiple factors of uncertainty, such as the charging/discharging plan of EVs, the capacity and type of EV batteries, the proportion of EVs in parking lots, driver behavior, EV arrival/departure timings, and the SOC of the batteries. In this paper, the total capacity of PLs is assumed to be 500 EVs [34]. The scheduling of EV arrival and departure times is represented by the

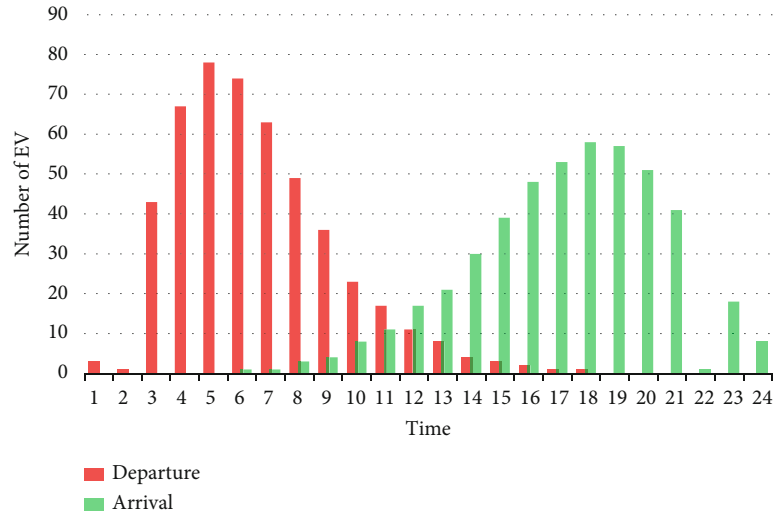

Figure 3: The EVs of arrival and their departure.

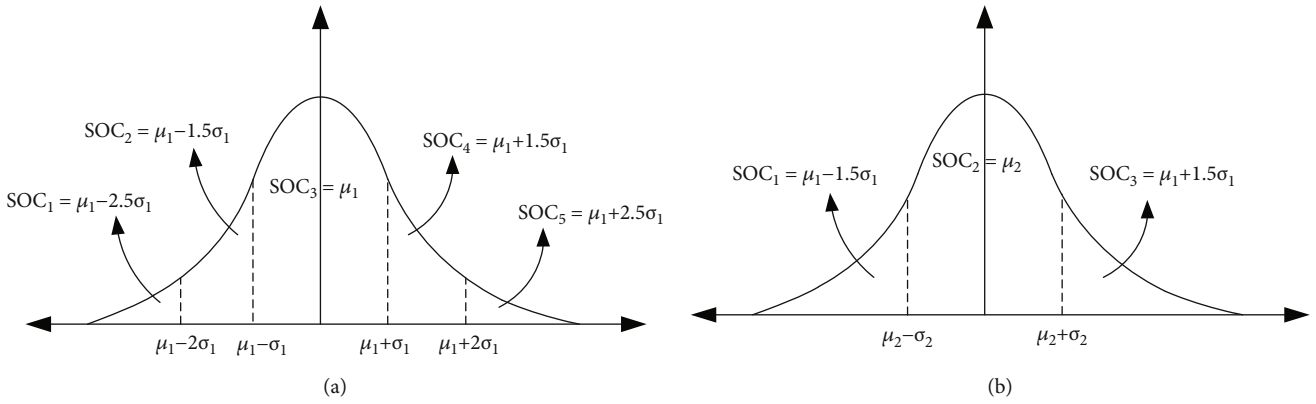

Figure 4: (a) The initial battery charging PDF. (b) The charging and discharging ratio PDF.

Weibull and Lognormal probability distribution functions, respectively. The parameters of the PDFs are listed in Table 1. The Weibull PDF and Lognormal PDF are represented by equations (24) and (25), respectively [35].

$$f_{t,h}^{\text{arr}} = \frac{k}{\Omega}\left(\frac{t}{\Omega}\right)^{k-1} e^{-(t/\Omega)^k}, \quad 0 < t < 24, \tag{24}$$

$$f_{t,h}^{\text{dep}} = \frac{1}{t\sigma\sqrt{2\pi}} e^{-(\ln t-\mu)^2/2\sigma^2}, \quad 0 < t < 24, \tag{25}$$

where $f_{t,h}^{\text{arr}}$ and $f_{t,h}^{\text{dep}}$ represent the Weibull PDF and Lognormal PDF for the EV's arrival and departure, respectively.

Figure 3 illustrates the amount of EV arrivals and their departures, based on the parameters of the probability density functions (PDFs) [35].

The initial conditions of battery charging are influenced by several factors, such as distance traveled, kind of the EV battery, and its efficiency. Due to the variations in these parameters across EVs, the remaining energy in the batteries can be calculated probabilistically. This study encompasses three modes of charging and discharging ratio. The initial battery charge and the nominal charging and discharging ratios are selected based on the obtained scenario from Figure 4 PDFs. The scenario distribution curves presented in this approach are categorized into three zones for the initial SOC and five zones for the charge/discharge ratio.

Table 2: The SOC and charging rate parameters [36].

	SOC		Maximum charge\discharge rate
	Discharge mode	Discharge mode	
Mean	72	26	10
μ	2.6	1.7	1.1

It is worth mentioning that the PDF curve is estimated using the information provided in Table 2.

It is assumed that the initial charge and charging and discharging ratio are considered independent of one another. Therefore, the scenarios are combined in order to

generate a comprehensive scenario, based on equation (26). These scenarios are shown in Table 3.

$$\pi^{S} = \pi^{\mathrm{EV}} \times \pi^{\mathrm{SOC}}. \tag{26}$$

In this equation, π^{EV} represents the probabilities associated with the charging and discharging ratio. Additionally, π^{SOC} denotes the probability of the initial SOC in scenarios.

Equations (27) and (28) can be used to calculate the needed time for full charging or full discharging of the EV battery depending on the initial SOC:

$$t_{\mathrm{charge}}(s,n) = \frac{(\mathrm{SOC}^{\max} - \mathrm{SOC}_{n,s}) \times \mathrm{ES}_n}{P_{V_s}}, \tag{27}$$

$$t_{\mathrm{discharge}}(s,n) = \frac{\left(\mathrm{SOC}_{s,n} - \mathrm{SOC}^{\min}\right) \times \mathrm{ES}_n}{P_{V_s}}. \tag{28}$$

Equation (29) can be employed to compute the anticipated input and output power generated by the j^{th} parking lot within each Monte Carlo simulation. In this equation, $\mathrm{SOC}^{\max}$ is the maximum charging level and $\mathrm{SOC}^{\min}$ represents the minimum charging level of the EV battery. ES_n indicates the capacity of the battery, and P_v represents the maximum charging and discharging ratio of the EVs. Therefore, the anticipated input and output power of the j^{th} parking lot at the demand level h in each Monte Carlo test (e) can be calculated using the following equation [37]:

$$P_{h,j}^{\mathrm{PL},e} = \sum_{s=1}^{N_S} \sum_{n=1}^{N_{\mathrm{EV}j}} \mathrm{CP}_j \times P_{V_s} \times \mathrm{SOC}_{s,n}, \tag{29}$$

where CP_j is the amount of parked electric vehicles in the PL, $M_{h,j}^{e}$ is the percentage of the EVs present in the PL at the demand level h, and also $\mathrm{SOC}_{s,n}$ is the initial SOC of an electric vehicle. $N_{\mathrm{EV}j}$ is the amount of EVs in the PL. Also, $\mathrm{SOC}^{\min}$ is 20% and $\mathrm{SOC}^{\max}$ is 80%.

3.2. Monte Carlo Simulation. In this research, the Monte Carlo simulation (MCS) is employed to generate the required scenarios for energy management within the microgrid.

The MCS is a stochastic approach employed to predict the behavior of components within the MG. The following are the essential stages involved in estimating uncertainty using the MCS [38, 39]:

Step 1. Develop the mathematical representation of the measurement.

It is necessary to establish the mathematical equation among the quantification outputs (Y) and the inputs (X_i).

$$Y = f(X_1, X_2, \cdots, X_n). \tag{30}$$

Step 2. Assign PDFs to the inputs.

Table 3: The scenarios of initial SOC and charging/discharging ratio along with their associated probabilities.

	SOC	Charge and discharge ratio	(π_s)
S1	$\mu_1 - 2.5\sigma_1$	$\mu_2 - 1.5\sigma_2$	0.0035
S2	$\mu_1 - 1.5\sigma_1$	$\mu_2 - 1.5\sigma_2$	0.0182
S3	μ_1	$\mu_2 - 1.5\sigma_2$	0.0966
S4	$\mu_1 + 1.5\sigma_1$	$\mu_2 - 1.5\sigma_2$	0.0182
S5	$\mu_1 + 2.5\sigma_1$	$\mu_2 - 1.5\sigma_2$	0.0035
S6	$\mu_1 - 2.5\sigma_1$	μ_2	0.018
S7	$\mu_1 - 1.5\sigma_1$	μ_2	0.0936
S8	μ_1	μ_2	0.4936
S9	$\mu_1 + 1.5\sigma_1$	μ_2	0.0936
S10	$\mu_1 + 2.5\sigma_1$	μ_2	0.018
S11	$\mu_1 - 2.5\sigma_1$	$\mu_2 + 1.5\sigma_2$	0.0035
S12	$\mu_1 - 1.5\sigma_1$	$\mu_2 + 1.5\sigma_2$	0.0182
S13	μ_1	$\mu_2 + 1.5\sigma_2$	0.0966
S14	$\mu_1 + 1.5\sigma_1$	$\mu_2 + 1.5\sigma_2$	0.0182
S15	$\mu_1 + 2.5\sigma_1$	$\mu_2 + 1.5\sigma_2$	0.0035

Considering the PDFs for the input (X_i), the inputs are independent.

Step 3. Obtain the PDFs for the outputs.

A significant random value (M) is generated for each input based on its respective distribution function. These generated random values for each input are subsequently fed into the mathematical model of the measurement system. By employing the mathematical models, the corresponding M value is obtained as the output variable. Ultimately, by utilizing the computed values, the probability density function of the output variable can be determined.

Step 4. Estimate the uncertainty of the measurement.

During this stage, the PDF of the output quantity (Y) is utilized to calculate the mathematical expectation of Y (estimated value of the output quantity). The standard deviation of Y is determined as a measure of the standard uncertainty associated with the output variable. Additionally, the certitude distance, taking into account Y, is determined to specify the probability.

The advantages of using the MCS method include:

(i) No knowledge of the exact value of the transfer function f is required in the MCS to calculate Y. This allows the problem to be treated as a black box that accepts samples and produces the corresponding output

(ii) The MCS performs effectively in complex and high-level systems

(iii) The MCS accommodates various types of probability density functions

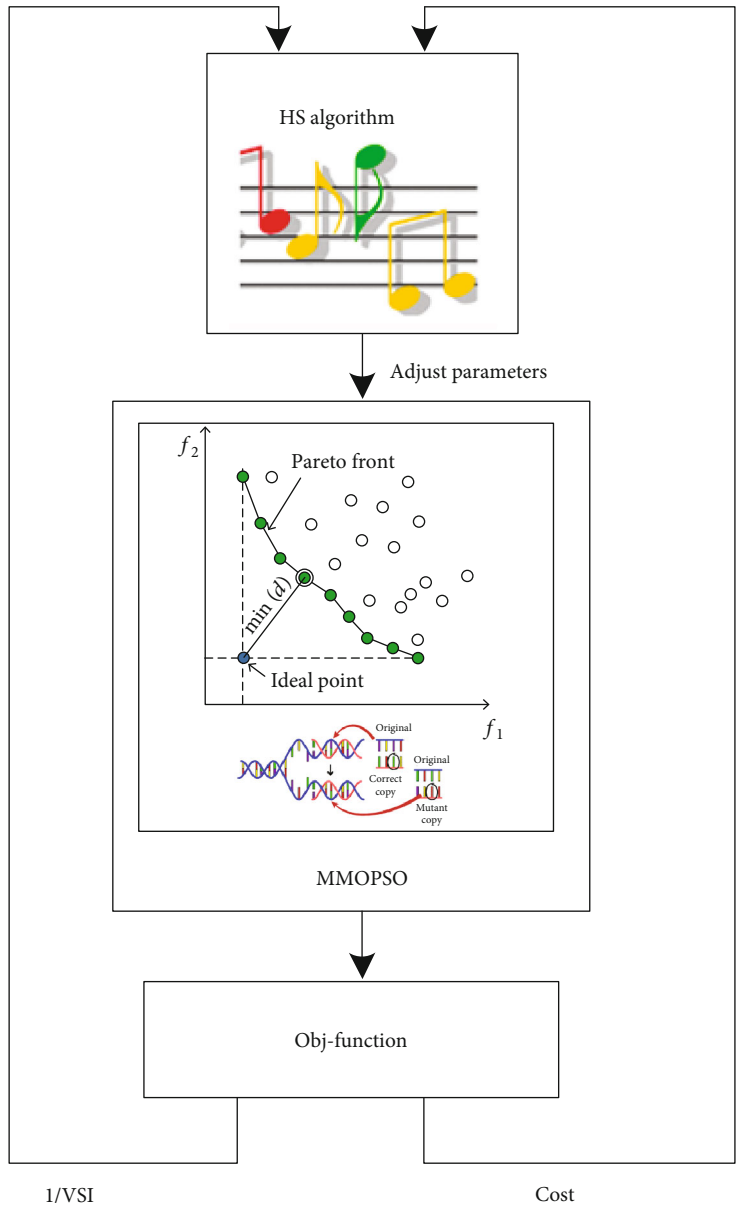

Figure 5: The hMOPSO-HS algorithm mechanism.

(iv) The MCS is simple and easy to implement

4. Proposed Optimization Algorithm

The proposed hMOPSO-HS algorithm is a combination of the MOPSO and HS algorithms. In the proposed algorithm, genetic mutations are applied to the MOPSO algorithm and subsequently, during each iteration of the algorithm, the parameters are effectively fine-tuned using the harmony search algorithm. The mechanism of the proposed algorithm is shown in Figure 5.

The multiobjective particle swarm optimization algorithm is a modified version of the PSO algorithm, initially proposed. In this algorithm, particles are initially scattered randomly throughout the search space, and objective functions are computed for all the particles. Following that, the particles are assessed based on their results, and the nondominated particles are retained in a repository. The particle's positions are updated according to the following equations:

$$\begin{aligned} V_k(t+1) &= D_d \times w \times v_k(t) + c_1 \times r_1 \\ &\quad \times \left(x_k^{\text{Pbest}}(t) - x_k(t)\right) + c_2 \times r_2 \\ &\quad \times \left(\text{Rep}_k(t) - x_k(t)\right), \\ x_k(t+1) &= x_k(t) + v_k(t+1), \end{aligned} \tag{31}$$

where v_k is the particle velocity, D_d is the damping coefficient, w is the weighting factor, and r_1 and r_2 represent

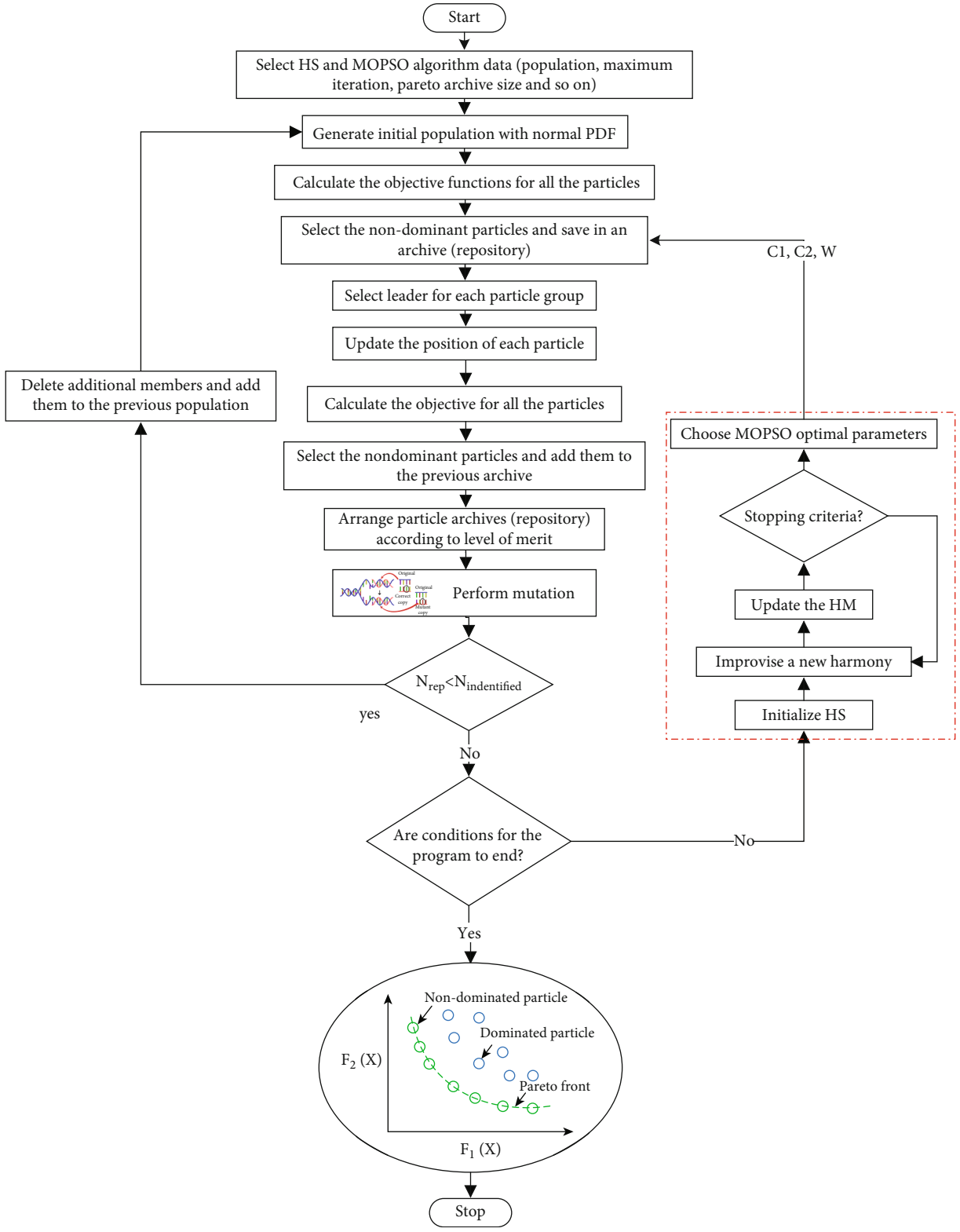

Figure 6: The proposed hMOPSO-HS algorithm flowchart.

random values ranging from 0 to 1. Also, c_1 and c_2 are impression coefficients and $\text{Rep}_k(t)$ represents a chosen solution from the repository. For the following iterations, the ${x_k}^{\text{Pbest}}(t)\,(t)$ is updated using the following procedure:

(1) If $x_k(t+1)$ dominates ${x_k}^{\text{Pbest}}(t)$, then ${x_k}^{\text{Pbest}}(t+1) = x_k(t+1)$

(2) If the current dominates $x_k(t+1)$, then ${x_k}^{\text{Pbest}}(t+1) = {x_k}^{\text{Pbest}}(t)$

Start
- Select the hMOPSO-HS algorithm parameters
- Initialize the HS population. (Select randomly *C1, C2 and* ω)
- **While** Iter1< Maximum Iteration
- **For all** HS populations **do**
- Initialize the MOPSO population.
- Calculate objective functions for all the particles.
- Select non-dominated populations and store them in the repository.
- Choose the best result.
- **While** Iter2< Maximum Iteration
- **For all** MOPSO particles **do**
- Update C1, C2, ω.
- Update MOPSO population positions.
- Choose a non-dominated population and update the repository.
- Find the best result.

  end for
- Iter2=Iter2+1;
- **end while**
- Improvise new harmony
- Update HM
- **end for**
- Iter1=Iter1+1;
- **end while**

End

Algorithm 1: The pseudocode of the proposed hMOPSO-HS algorithm.

(3) If no clear dominance exists among the solutions, a random selection is made to determine the $x_k^{P\text{best}}(t+1)$ from the available options

These stages is repeated till the best solution is achieved. For the mutated version of the MOPSO algorithm, genetic mutation is used for the number of particles. Thus, the PM% (percent of mutation) of the particles that are not in the repository are selected for making mutations as equation (32). It is recommended that the PM be selected less than 25%.

$$x_k(t+1) = x_k(t) + M_f \times r \times (\max_{\text{val}} - \min_{\text{val}}), \tag{32}$$

where r represents a randomly generated number following a normal distribution, $\max_{\text{val}}$ and $\min_{\text{val}}$ are variable upper and lower limits, respectively, and M_f is the mutation rate.

In the hMOPSO-HS algorithm, the harmonic search (HS) algorithm is used for accurate estimation of the MOPSO parameters. The HS algorithm is inspired by the collaborative behavior of musicians during music production. The harmonic search algorithm defines a harmonic memory that contains a finite set of better harmonies (responses). This space is defined as a matrix called the harmonic memory matrix. After the initial formation of harmonic memory, the response vectors are arranged according to the results for these vectors. The general form of this memory matrix is as follows [40]:

$$\text{HM} = \begin{bmatrix} x^1 \\ x^2 \\ \vdots \\ x^{\text{HMS}} \end{bmatrix} = \begin{bmatrix} x_1^1 & x_2^1 & \cdots & x_N^1 \\ x_1^2 & x_2^2 & \cdots & x_N^2 \\ \vdots & \vdots & \ddots & \vdots \\ x_1^{\text{HMS}} & x_1^{\text{HMS}} & \cdots & x_N^{\text{HMS}} \end{bmatrix}. \tag{33}$$

To create a value for the i variable, first, a random number between zero and one is generated. This random number is compared to the HMCR, and if it is smaller than that, a value for the i variable is selected from the memory matrix and the i column. Otherwise, a random amount of search space is selected for the i variable. If a value is selected from the memory matrix, then another random number is generated and compared to PAR. If the random number is less than PAR, the selected variable from the memory matrix is changed to a small value according to the following equation. To determine the amount of change in the variable selected from the matrix memory, another parameter called $b\omega$ is defined, which is obtained according to the value of the new variable:

$$x_k(t+1) = x_k(t) + b\omega + \varepsilon. \tag{34}$$

In the same way, all variables of a harmony are created and then the value of that harmony is calculated according to the objective function, and they are compared with the worst harmony in the matrix memory. If it is better than the worst harmony in the matrix memory, the new harmony is replaced with the previous one. The condition for stopping the algorithm is to achieve maximum iteration. The

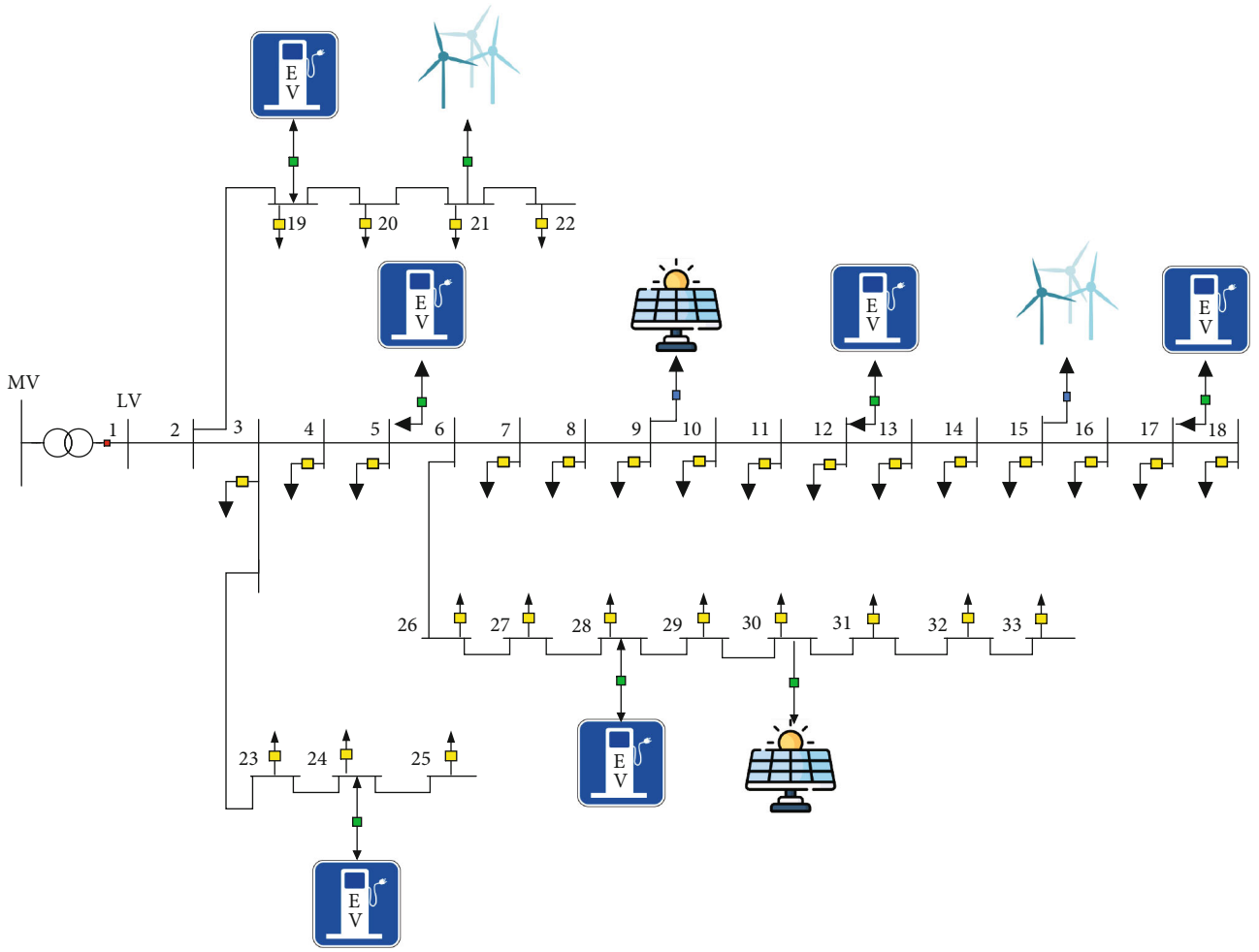

Figure 7: The modified IEEE 33-bus network.

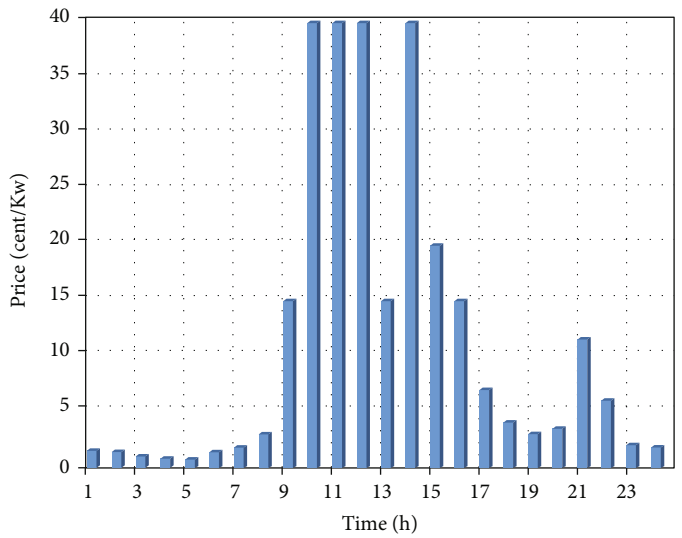

Figure 8: The per-hour electricity price [45].

Table 4: The IGD index values for the unconstrained benchmark functions.

	UF1	UF2	UF3	UF4	UF5	UF6	UF7	UF8	UF9	UF10
hMOPSO-HS	0.005743	0.004373	0.048562	0.053022	0.071675	0.062543	0.05348	0.061612	0.057973	0.180345
MOPSO	0.006115	0.005784	0.043003	0.049105	1.930803	0.610471	0.008268	0.236419	0.175671	0.526617
MOABC [47]	0.00618	0.00484	0.0512	0.05801	0.077758	0.06537	0.05573	0.06726	0.0615	0.19499
MOEAD [47]	0.00435	0.00679	0.00742	0.06385	0.18071	0.00587	0.00444	0.0584	0.07896	0.47415
GDE3 [47]	0.00534	0.01195	0.10639	0.0265	0.03928	0.25091	0.02522	0.24855	0.08248	0.43326
MOEADGM [47]	0.0062	0.0064	0.0429	0.0476	1.7919	0.5563	0.0076	0.2446	0.1878	0.5646
MTS [47]	0.00646	0.00615	0.0531	0.02356	0.01489	0.05917	0.04079	0.11251	0.11442	0.15306
LiuLi algorithm [47]	0.00785	0.0123	0.01497	0.0435	0.16186	0.17555	0.0073	0.08235	0.09391	0.44691

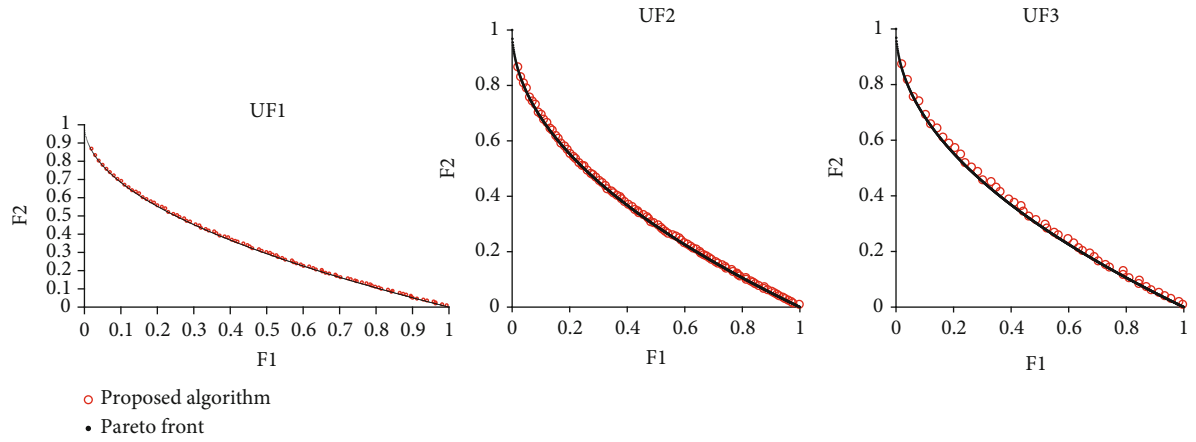

Figure 9: Pareto fronts of the proposed algorithm for the UF functions.

Table 5: The IGD index values for the constrained benchmark functions.

	CF1	CF2	CF3	CF4	CF5	CF6	CF7
hMOPSO-HS	0.005743	0.004373	0.048562	0.053022	0.071675	0.062543	0.05348
MOPSO	0.006115	0.005784	0.043003	0.049105	1.930803	0.610471	0.008268
MOABC [47]	0.00992	0.01027	0.08621	0.00452	0.06781	0.00483	0.01692
GDE3 [47]	0.0294	0.01597	0.1275	0.00799	0.06799	0.06199	0.04169
MOEADGM [47]	0.0108	0.008	0.5134	0.0707	0.5446	0.2071	0.5356
MTS [47]	0.01918	0.02677	0.10446	0.01109	0.02077	0.01616	0.02469
LiuLi algorithm [47]	0.00085	0.0042	0.1829	0.01423	0.10973	0.01394	0.10446

schematic diagram illustrating the MOPSO-HS algorithm is depicted in Figure 6.

The pseudocode of the proposed hMOPSO-HS algorithm is given in Algorithm 1.

5. The Understudy Microgrid

Figure 7 illustrates the test system employed as a microgrid (MG) in this study [41–43]. The understudy microgrid incorporates two 500 kW WTs located at bus 15 and bus 21, as well as two 500 kW PV arrays situated at buses 9 and 30. Furthermore, the MG includes six 500 kW parking lots positioned at buses 5, 12, 17, 19, 24, and 28. The wind velocity and irradiation data utilized in the analysis are obtained from the McHenry precinct of the North Dakota region [44]. Moreover, the load flow calculations are carried out using the forward-backward sweep (FBS) method.

An energy management period of 24 hours is carried out to facilitate the charging and discharging operations of EVs. The power exchange between PLs and the MG involves a total of 500 EVs. These EVs are assumed to be of the Chevrolet model, based on the technical specifications provided in [44]. Each EV has a battery capacity of 16 kWh, and the maximum charging and discharging power for each EV is set at 5 kW. The electricity prices procured from the upstream network for each hour are illustrated in Figure 8 [45].

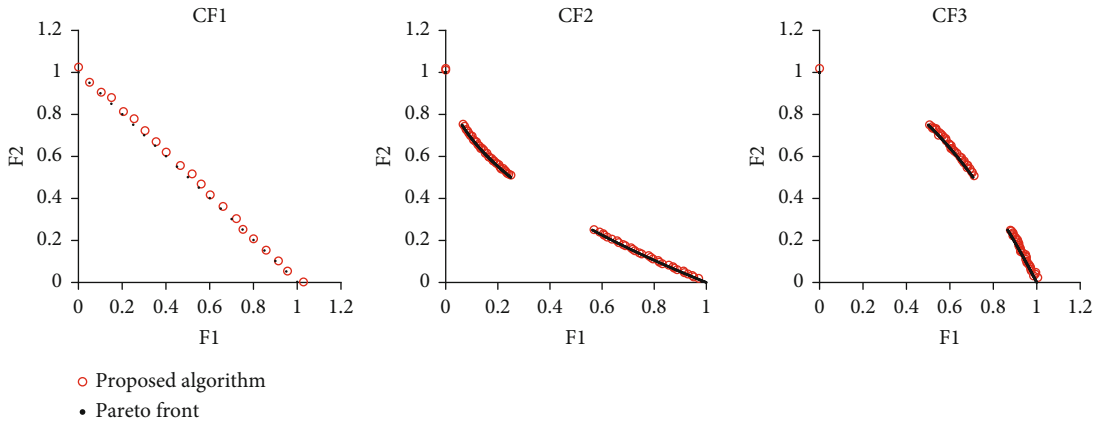

Figure 10: Pareto fronts of the proposed algorithm for the CF functions.

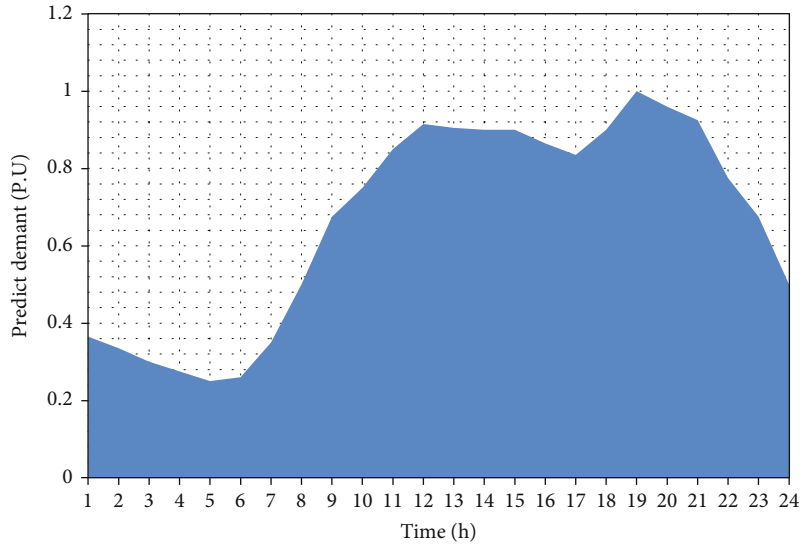

Figure 11: The predicted electrical demand [45].

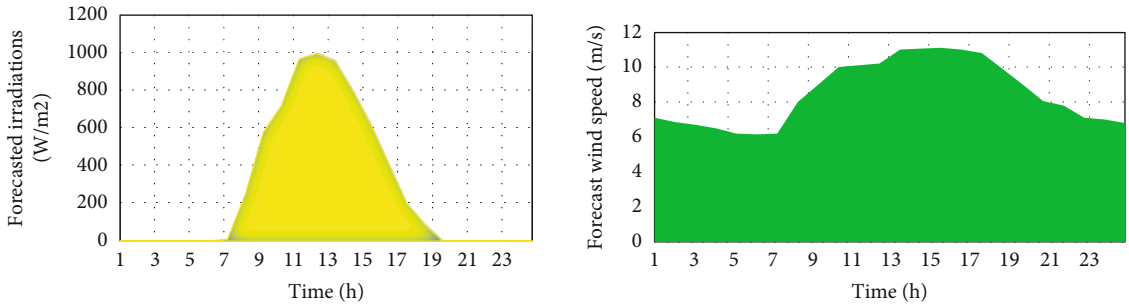

Figure 12: Forecasted irradiation intensity and wind speed [43].

6. Simulation Results Analysis

The simulations are performed in three parts. Firstly, the performance of the hMOPSO-HS algorithm is assessed by conducting optimization on several benchmarks. In the second part, the simulation is done regardless of the uncertainties and with the predicted definite data, and in the third part, the uncertainty is considered by selecting 15 scenarios from the MCS. To achieve the optimal energy management of MG in two cases, multiobjective particle swarm optimization (MOPSO) algorithm, nondominated sorting genetic algorithm (NSGAII), multiobjective differential evolution (MODE), multiobjective gray wolf optimization (MOGWO), and also the hMOPSO-HS algorithm is used.

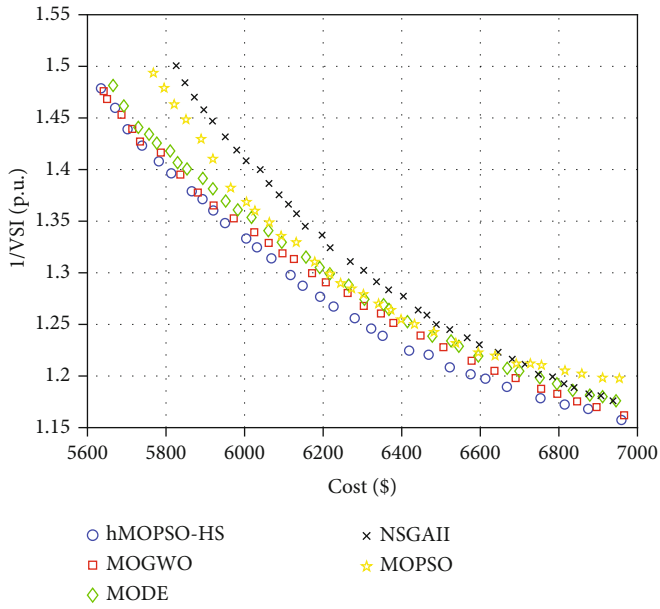

Figure 13: Pareto fronts of the algorithms in the first section of the simulation.

6.1. First Section of the Simulation Results (Algorithm Performance Evaluation). In this part, the hMOPSO-HS performance is assessed by conducting optimization on the CEC′09 benchmark functions [46]. The optimization process covers both unconstrained test functions UF1–UF10 and constrained test functions CF1–CF7 using the hMOPSO-HS algorithm. The acquired outcomes are subsequently contrasted with diverse multiobjective algorithms. The performance assessment is based on the calculation of the inverse generational distance (IGD). Smaller values of the IGD index indicate a smaller discrepancy between the values of the actual Pareto front and the Pareto front obtained through the optimization algorithm. After solving UF1-UF10, the corresponding IGD values were calculated and presented in Table 4.

The lower values of IGD indicate the superior performance of the proposed hMOPSO-HS algorithm in finding optimal solutions. Figure 9 displays the Pareto front for UF1 to UF3.

As depicted in Figure 9, the Pareto front obtained by the hMOPSO-HS algorithm exhibits minimal deviations from the actual Pareto front. Subsequently, the proposed MOGOA-BES algorithm was employed to optimize the constrained test functions (CF1-CF7), and the corresponding IGD index values are calculated and presented in Table 5.

The lower values of the IGD index in solving CF problems validate the higher accuracy and suitable dispersion of the solutions obtained by the proposed algorithm in comparison to other algorithms. Figure 10 illustrates the Pareto fronts of the proposed algorithm and the actual Pareto fronts for CF1, CF2, and CF3.

6.2. Second Section of the Simulation Results (Regardless of Uncertainty). For the first part of the simulation, uncertainty is not considered, and definite data are used to perform the optimization. The predicted electrical demand by customers is shown in Figure 11.

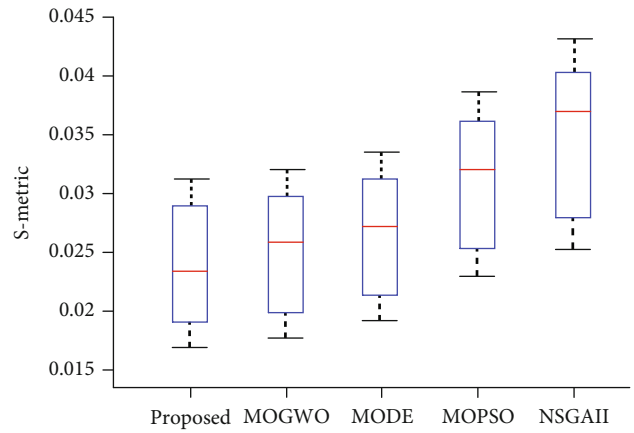

Figure 14: The S-metric criterion for the first section.

Table 6: The optimal results in the first section.

	NSGAII	MOPSO	MODE	MOGWO	hMOPSO-HS
Cost ($)	6269	6235	6234	6230	6203
1/VSI (p.u.)	1.321	1.287	1.287	1.282	1.274

The projected values of irradiation and wind speed are illustrated in Figure 12. The PV system unit has the capability to generate electricity between 8 am and 6 pm, while no power generation occurs during the remaining hours due to insufficient solar irradiation. The wind speed in the specified area fluctuates between 6 m/s and 11 m/s [47].

The Pareto fronts for the optimization algorithm are depicted in Figure 13.

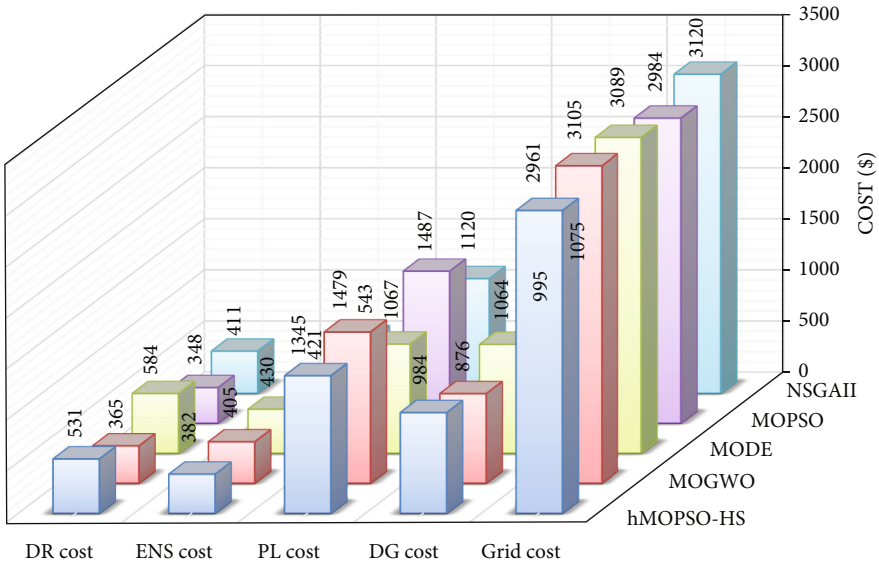

Figure 15: The MG operation cost separately.

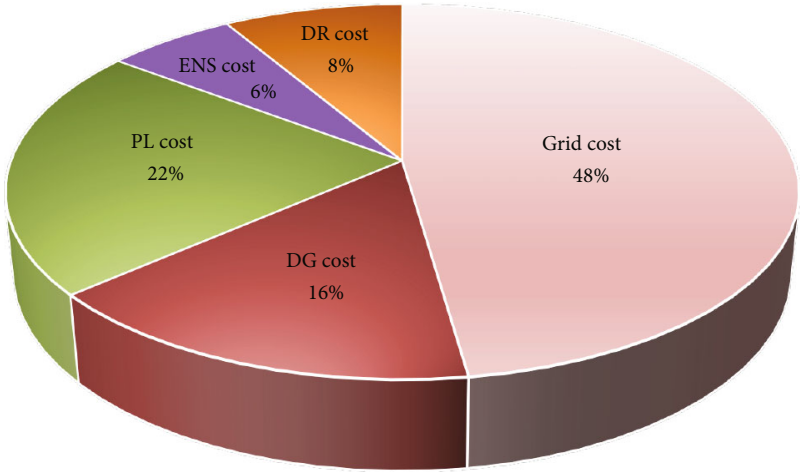

Figure 16: Percentage share of each component in the MG operation cost.

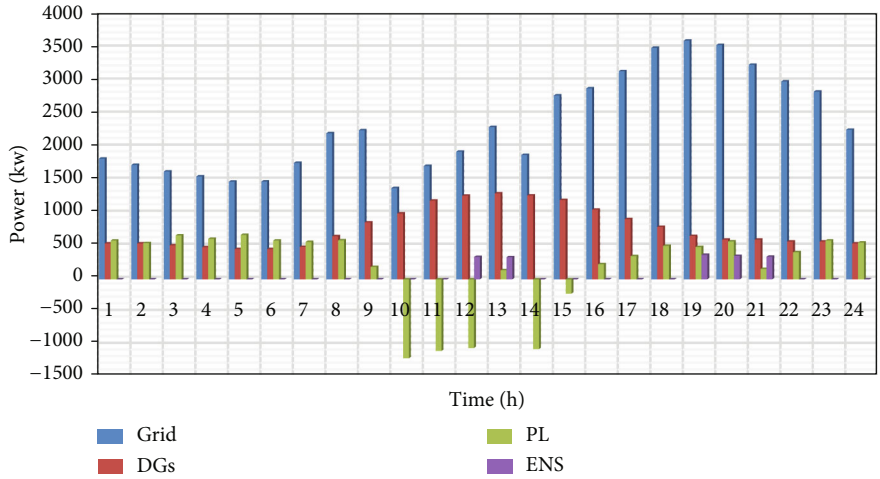

Figure 17: The active power of each MG component.

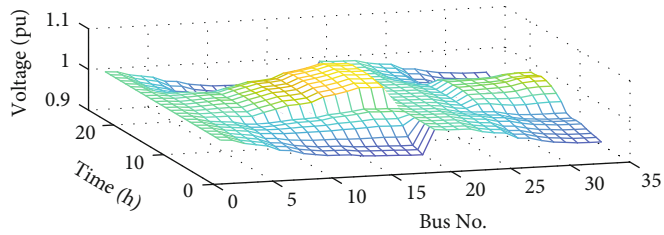

Figure 18: The MG voltage profile.

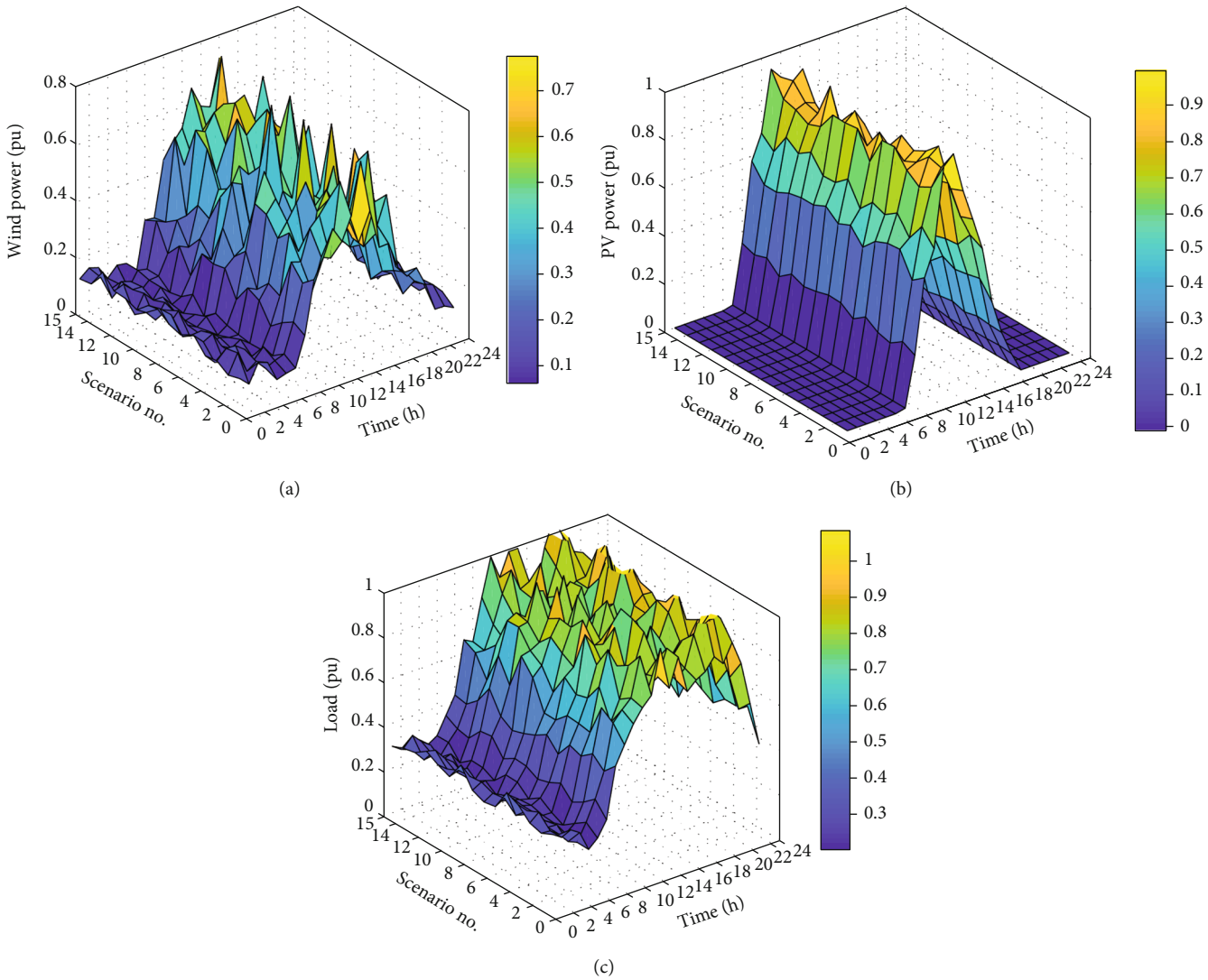

Figure 19: Generation and demand for 15 scenarios.

To assess the optimization outcomes, the S-metric index is computed to gauge the dispersion of the dominating particles, and its representation can be observed in Figure 14. A smaller amount of the mean metric distance signifies that the Pareto particles are more scattered, and zero values of the S-metric distance mean that all the dominant particles are distributed at the same Pareto distance.

The best result is selected from the dominant particles. Also, the fuzzy mechanism is used for the best results selection. The optimal outcomes for the optimization algorithms are presented in Table 6.

Based on the findings presented in Table 6, it can be observed that the hMOPSO-HS algorithm outperformed other metaheuristic algorithms in terms of performance.

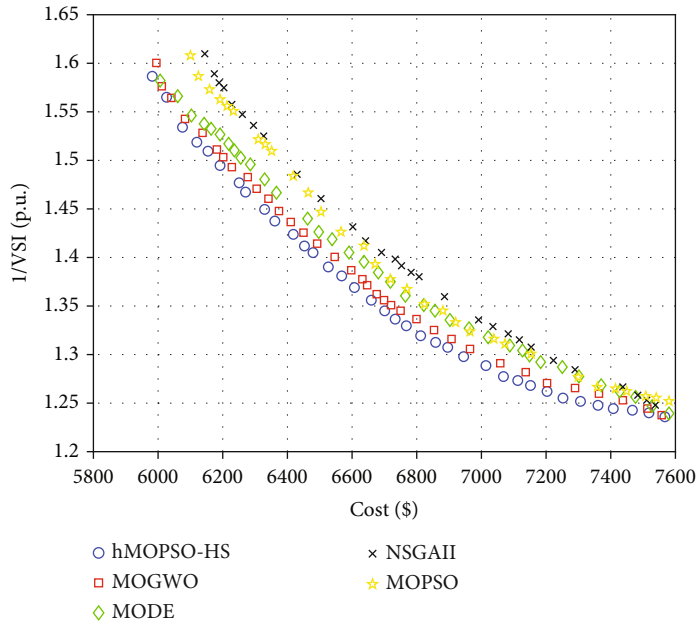

Figure 20: Pareto fronts of the algorithms in the second part.

The final cost for the hMOPSO-HS is $6203 and the voltage stability index in the MG is 1.274 p.u. Figure 15 shows the operating cost of the MG separately.

To better analyze the performance of the hMOPSO-HS optimization algorithm on MG operation costs, the share of each component in the final cost is shown as a percentage in Figure 16. About 48% of the MG operation cost is allocated to the purchase of electricity from the upstream network, while the share of distributed generation and parking lots from the final cost of operation is 16% and 22%, respectively. The DR share is equal to 8%, and the ENS fine share is about 6% of the final cost.

Figure 17 shows the generation capacity of each part of the MG components for 24 hours after optimization by the proposed hMOPSO-HS algorithm.

In this case, the MG voltage profile in 24 hours is shown in Figure 18. The voltage amplitude in all buses for 24 hours is more than 0.94 p.u.

6.3. Third Section of the Simulation Results (considering Uncertainty). In the second section of the simulations, demand and generation uncertainties as well as parking lot uncertainties are considered. Fifteen scenarios are chosen by the MCS, and the per-unit values of wind power, PVs and charge in these scenarios are shown in Figure 19.

The Pareto fronts for the optimization algorithms in the second part are shown in Figure 20.

Similar to the first section, for better evaluation, the S-metric index is calculated for the algorithms which is shown in Figure 21.

Considering the uncertainty, the S-metric index results reveal an increase in the dispersion of the outcomes compared to the first section. A lower mean value of the S-metric index means scattering with a uniform distribution of dominant particles of the proposed hMOPSO-HS. The

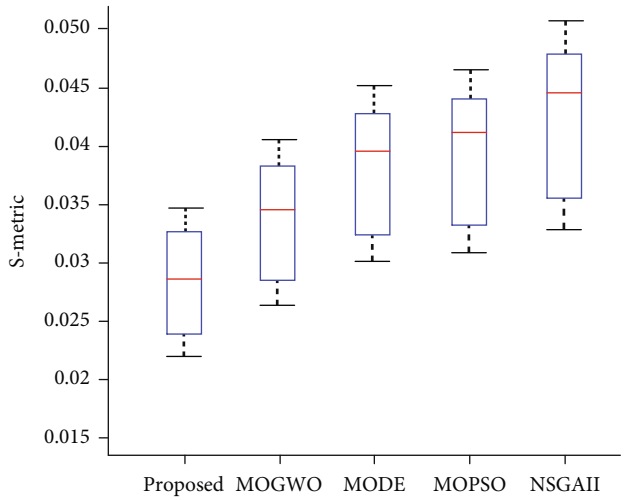

Figure 21: The S-metric index for the second section.

Table 7: The optimal results in the second section.

	NSGAII	MOPSO	MODE	MOGWO	hMOPSO-HS
Cost ($)	6684	6673	6623	6646	6605
1/VSI (p.u.)	1.412	1.388	1.391	1.371	1.367

MG cost and the voltage stability function for the selected particles are given in Table 7.

In this section, the MG operation cost and 1/VSI index are the lowest when the proposed hMOPSO-HS is used for MG energy management. The operation cost is $6605, and 1/VSI is 1.367 p.u. for the MG optimized by the hMOPSO-

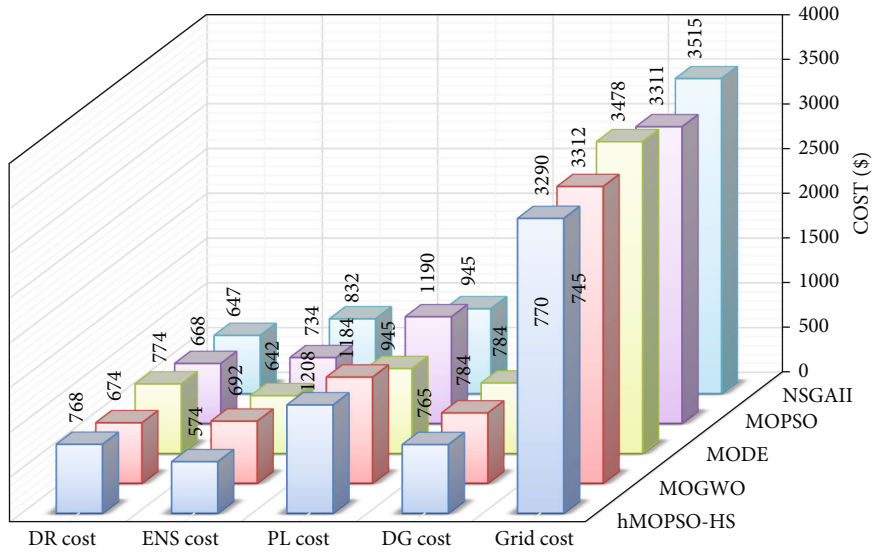

Figure 22: Detailed MG operation cost in the presence of uncertainty.

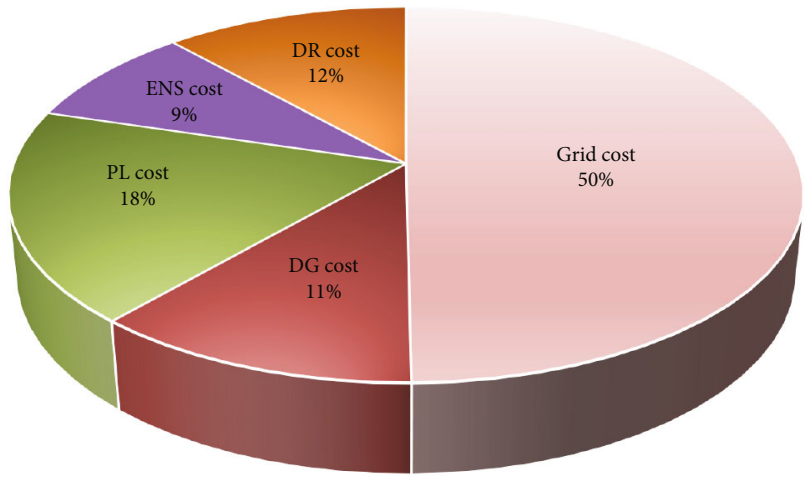

Figure 23: Percentage share of each component in the MG operation cost in the presence of uncertainty.

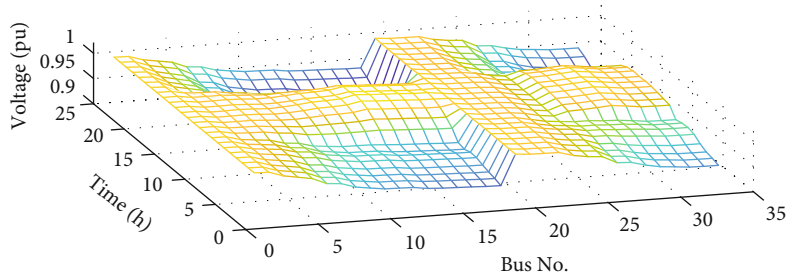

Figure 24: The MG voltage profile in case of uncertainty.

HS. In Figure 22, the MG component cost is shown as a separate bar chart. The results show that considering the uncertainty in MG, it increases the purchasing energy cost from the power grid and the penalty for not supplying energy. Also, the demand response program has played an important role in reducing operation costs.

In Figure 23, the share of each part in the final cost is shown by percentage.

In this part of the simulation, the percentage of the cost from a power system is about 50% and it has increased by 2% compared to conditions without considering uncertainty. Also, the share of ENS and DR has increased. The DR share

of total cost is 12%, and the ENS share is 9% for this section. But, the share of PL costs and DG production costs has decreased to 18% and 11%, respectively. The MG voltage is shown in Figure 24.

The voltage profile shows that in the case of uncertainties, the voltage amplitude has decreased compared to the conditions of the previous section. The minimum voltage amplitude is 0.93 p.u.

7. Conclusion

In this paper, a novel energy management system based on uncertainty for MG energy management is proposed. The MG selected for the simulation consists of PV and wind sources along with EV parking lots. The renewable source generation powers, PL, and load consumption uncertainties are considered in the simulation and other sources of uncertainty are omitted. The operation cost and voltage stability index (VSI) are considered objective functions, and an innovative hybrid algorithm called hMOPSO-HS is proposed for solving the optimization problem. The hMOPSO-HS algorithm is a combination of the mutant version of MOPSO and harmony search (HS) algorithms. Simulations are done in two different cases. In the first case, the uncertainty is neglected and, in the second part of the simulation, the uncertainty is considered. The optimization results of the proposed hMOPSO-HS algorithms are compared with several multiobjective algorithms for two cases of simulations and also the S-metric index is calculated for all of them. The simulation results indicate better performance of the hMOPSO-HS algorithm than all other algorithms. The simulation results also showed that if uncertainty is considered, the cost of the demand response program and the cost of purchasing energy from the upstream network will increase to reduce the impact of uncertainty on the sources of distributed generation and parking of EVs. For future studies, new electrical energy storage technologies such as compressed air storage (CAS) or power to gas (PtG) can be added to the microgrid and the impact of the presence of these storages can be investigated. Indeed, the studies presented in this paper can be replicated and applied to real-world systems. By conducting similar experiments on real systems, researchers can verify the effectiveness and applicability of the proposed approaches in practical scenarios.

Nomenclature

Abbreviations

DG: Distributed generation
DR: Demand response
DRP: Demand response program
ENS: Energy not supply
EMS: Energy management system
EV: Electric vehicles
hMOPSO-HS: Hybrid MOPSO-HS algorithm
HSA: Harmony search algorithm
MCS: Monte Carlo simulation
MG: Microgrid
MOPSO: Multiobjective particle swarm optimization
NLP: Nonlinear programming
PDF: Probability density functions
PL: Parking lot
PV: Photovoltaic
RTP: Real-time pricing
SOC: The state of charge
VSI: Voltage stability index
TOU: Time of use
WT: Wind turbine.

Parameters

α, β, and γ: Constant values for the DG
B_j^{charge}: Charging cost
$B_{t,h,j}^{\text{discharge}}$: Discharging cost
$P_{t,h}^{\text{LPSP}}$: Loss of supply probability
$P_{t,h}^{\text{UW}}$: Unwanted power interruption punishment
π_h: Probability of each sample
N_h: Number of random samples of operation conditions
$P_{t,h}^{\text{PV}}$: PV generated power
$P_{t,h}^{\text{WT}}$: WT generated power
$P^{\text{DG-max}}$: Maximum production capacity of DG
$P^{\text{DG-min}}$: Minimum production capacity of DG
u: Binary variable
$B_{t,n}$: Binary variables that show discharge mode
$P_n^{\text{charge-max}}$: Maximum charge rate of nth EV
$P_n^{\text{discharge-max}}$: Maximum discharge rate of nth EV
$E_{t,h,n}^{S}$: EV remaining energy
$E_{t,h,n}^{\text{trip}}$: EV traveling energy consumption
η_n^{charge}: Charging efficiency
$\eta_n^{\text{discharge}}$: Discharging efficiency
$\mu^{P^{\text{Load}}}$: Mean of load power
$\sigma^{P^{\text{Load}}}$: Variance of load power
si: Radiation intensity
A^{pv}: Size of the PV panel
η^{pv}: Efficiency of the PV panel
$G_{t,h}$: Solar irradiation
G^{STC}: Standard irradiation
$T_{t,h}$: Panel temperature
T^{STC}: Standard temperature
P^r: WT rated power
$si_{t,h}$: A random variable representing the intensity
μ^{υ}: Mean of wind data
σ^{υ}: Variance of wind data
$\upsilon(t)$: Wind speed
$\upsilon^{\text{cut-in}}$: Cut-in speed
$\upsilon^{\text{cut-out}}$: Cut-off speed
υ^r: Nominal speed
vk: Velocity of particle
D_d: Damping coefficient
w: Weighting factor
Rep: Repository
PM: Percent of mutation

HM: Harmony memory
$P_{t,h}^{\text{grid}}$: The energy exchanged to the network
$P^{\text{grid-max}}$: Maximum power exchanged with the network
$A_{t,n}$: Binary variables that show charge mode.

Data Availability

The data used to support the findings of this study are included within the article.

Conflicts of Interest

The authors declare that they have no conflicts of interest.

References

[1] M. Mohammadi, S. Soleymani, T. Niknam, and T. Amraee, "Stochastic multi-objective distribution automation strategies from reliability enhancement point of view in the presence of plug in electric vehicles," *IFAC-Papers Online*, vol. 36, no. 3, pp. 2933–2945, 2019.

[2] R. M. Azevedo, L. N. Canha, V. J. Garcia, C. A. S. Rangel, T. A. S. Santana, and Z. I. Nadal, "Dynamic and proactive matheuristic for AC/DC hybrid smart home energy operation considering load, energy resources and price uncertainties," *International Journal of Electrical Power & Energy Systems*, vol. 137, article 107463, 2022.

[3] M. S. Islam, "Coordinated EV charging for correlated EV and grid loads and PV output using a novel, correlated, probabilistic model," *International Journal of Electrical Power & Energy Systems.*, vol. 104, no. 1, pp. 335–348, 2019.

[4] Y. Hu and R. A. de Callafon, "Modeling microgrid power flow dynamics with covariance based realization," *International Journal of Electrical Power & Energy Systems*, vol. 153, p. 109279, 2023.

[5] E. Mirmoradi and H. Ghasemi, "Market clearing with probabilistic spinning reserve considering wind uncertainty and electric vehicles," *International Transactions on Electrical Energy Systems*, vol. 26, no. 3, pp. 525–538, 2016.

[6] R. Sabzehgar, M. A. Kazemi, M. Rasouli, and P. Fajri, "Cost optimization and reliability assessment of a microgrid with large-scale plug-in electric vehicles participating in demand response programs," *International Journal of Green Energy.*, vol. 17, no. 2, pp. 127–136, 2020.

[7] O. Rahbari, M. Vafaeipour, N. Omar et al., "An optimal versatile control approach for plug-in electric vehicles to integrate renewable energy sources and smart grids," *Energy*, vol. 134, no. 1, pp. 1053–1067, 2017.

[8] H. Shan, W. Zhensheng, R. Zhigang et al., "Multi-objective economic optimization operation of electric vehicle-contained microgrid based on cogeneration," *IEEE International Electrical and Energy Conference (CIEEC)*, vol. 4, no. 1, pp. 331–337, 2018.

[9] Z. Wang, Q. Zhu, M. Huang, and B. Yang, "Optimization of economic/environmental operation management for microgrids by using hybrid fireworks algorithm," *International Transactions on Electrical Energy Systems.*, vol. 27, no. 12, article e2429, 2017.

[10] B. Y. Qu, Y. S. Zhu, Y. C. Jiao, M. Y. Wu, P. N. Suganthan, and J. J. Liang, "A survey on multi-objective evolutionary algorithms for the solution of the environmental/economic dispatch problems," *Swarm and Evolutionary Computation*, vol. 38, pp. 1–11, 2018.

[11] H. Hosseini and B. Tousi, "Optimal operation of DG-based micro grid (MG) by considering demand response program (DRP)," *Electric Power Systems Research*, vol. 167, no. 1, pp. 252–260, 2019.

[12] E. Akhavan-Rezai, M. F. Shaaban, E. F. El-Saadany, and F. Karray, "New EMS to incorporate smart parking lots into demand response," *IEEE Transactions on Smart Grid*, vol. 9, no. 2, pp. 1376–1386, 2016.

[13] O. M. Abdelwahab, A. A. Shalaby, and M. F. Shaaban, "An optimal resource allocation for future parking lots with charger assignment considering uncertainties," *Electric Power Systems Research*, vol. 200, p. 107455, 2021.

[14] Q. Chen, F. Wang, B. M. Hodge et al., "Dynamic price vector formation model-based automatic demand response strategy for PV-assisted EV charging stations," *IEEE Transactions on Smart Grid*, vol. 8, no. 6, pp. 2903–2915, 2017.

[15] K. Mahmud, M. J. Hossain, and J. Ravishankar, "Peak-load management in commercial systems with electric vehicles," *IEEE Systems Journal*, vol. 1, no. 99, pp. 1–11, 2018.

[16] H. A. Aalami and A. Khatibzadeh, "Regulation of market clearing price based on nonlinear models of demand bidding and emergency demand response programs," *International Transactions on Electrical Energy Systems*, vol. 26, no. 11, pp. 2463–2478, 2016.

[17] P. Aliasghari, B. Mohammadi-Ivatloo, M. Alipour, M. Abapour, and K. Zare, "Optimal scheduling of plug-in electric vehicles and renewable micro-grid in energy and reserve markets considering demand response program," *Journal of Cleaner Production*, vol. 186, no. 1, pp. 293–303, 2018.

[18] F. S. Gazijahani, H. Hosseinzadeh, A. A. Abadi, and J. Salehi, "Optimal day ahead power scheduling of microgrids considering demand and generation uncertainties," *9432017 Iranian Conference on Electrical Engineering (ICEE)*, 948 pages, Tehran, Iran, 2017.

[19] L. Ju, H. Li, J. Zhao, K. Chen, Q. Tan, and Z. Tan, "Multi-objective stochastic scheduling optimization model for connecting a virtual power plant to wind-photovoltaic-electric vehicles considering uncertainties and demand response," *Energy Conversion and Management*, vol. 128, pp. 160–177, 2016.

[20] N. Nikmehr, S. Najafi-Ravadanegh, and A. Khodaei, "Probabilistic optimal scheduling of networked microgrids considering time- based demand response programs under uncertainty," *Applied Energy*, vol. 198, no. 198, pp. 267–279, 2017.

[21] M. Tayyab, I. Hauer, and S. Helm, "Holistic approach for microgrid planning for e-mobility infrastructure under consideration of long-term uncertainty," *Sustainable Energy, Grids and Networks*, vol. 34, article 101073, 2023.

[22] M. Marzband, N. Parhizi, and J. Adabi, "Optimal energy management for standalone microgrids based on multi-period imperialist competition algorithm considering uncertainties: experimental validation," *International Transactions on Electrical Energy Systems*, vol. 26, no. 6, pp. 1358–1372, 2016.

[23] B. Khaki, Y. W. Chung, C. Chu, and R. Gadh, "Probabilistic electric vehicle load management in distribution grids," *IEEE Transportation Electrification Conference and Expo (ITEC)*, vol. 19, no. 1, pp. 1–6, 2019.

[24] M. Sedighizadeh, G. Shaghaghi-shahr, M. Esmaili, and M. R. Aghamohammadi, "Optimal distribution feeder reconfiguration and generation scheduling for microgrid day-ahead

operation in the presence of electric vehicles considering uncertainties," *Journal of Energy Storage*, vol. 21, pp. 58–71, 2019.

[25] J. Sarshar, S. Moosapour, and M. Joorabian, "Multi-objective energy management of a micro-grid considering uncertainty in wind power forecasting," *Energy*, vol. 139, pp. 680–693, 2019.

[26] S. Rajamand, "Cost reduction in microgrid using demand response program of loads and uncertainty modeling with point estimation method," *International Transactions on Electrical Energy Systems*, vol. 30, no. 4, article e12299, 2020.

[27] A. Ajoulabadi, S. N. Ravadanegh, and B. Mohammadi-Ivatloo, "Flexible scheduling of reconfigurable microgrid-based distribution networks considering demand response program," *Energy*, vol. 196, article 117024, 2020.

[28] H. Mehrjerdi, "Dynamic and multi-stage capacity expansion planning in microgrid integrated with electric vehicle charging station," *Journal of Energy Storage*, vol. 29, p. 101351, 2020.

[29] R. A. Thokar, N. Gupta, K. R. Niazi, A. Swarnkar, N. K. Meena, and V. C. Pandey, "A rational pricing model for demand response programs in contemporary distribution systems," *Sustainable Energy Technologies and Assessments*, vol. 56, article 103024, 2023.

[30] J. Kartite and M. Cherkaoui, "Optimal sizing of hybrid renewable PV/wind battery system using LPSP methods," in *2017 6th International Conference on Systems and Control (ICSC)*, pp. 226–230, Batna, Algeria, 2017.

[31] H. Shokouhandeh and M. Jazaeri, "An enhanced and autotuned power system stabilizer based on optimized interval type-2 fuzzy PID scheme," *International Transactions on Electrical Energy Systems*, vol. 28, no. 1, article e2469, 2018.

[32] A. Cabrera-Tobar, A. M. Pavan, N. Blasuttigh, G. Petrone, and G. Spagnuolo, "Real time energy management system of a photovoltaic based e-vehicle charging station using explicit model predictive control accounting for uncertainties," *Sustainable Energy, Grids and Networks*, vol. 31, article 100769, 2022.

[33] A. Ramadan, M. Ebeed, S. Kamel, and L. Nasrat, "Optimal allocation of hybrid solar-wind distributed generations in distribution networks considering the uncertainty using grasshopper optimization algorithm," in *2019 21st International Middle East Power Systems Conference (MEPCON)*, pp. 406–410, Cairo, Egypt, 2019.

[34] S. Guner, A. Ozdemir, and G. Serbes, "Impact of car arrival/departure patterns on EV parking lot energy storage capacity," in *2016 International Conference on Probabilistic Methods Applied to Power Systems (PMAPS)*, Beijing, China, 2016.

[35] M. Nodehi, A. Zafari, and M. Radmehr, "A new energy management scheme for electric vehicles microgrids concerning demand response and reduced emission," *Sustainable Energy, Grids and Networks*, vol. 32, article 100927, 2022.

[36] K. Nasraoui, N. Lakhoua, and L. E. Amraoui, "Study and analysis of micro smart grid using the modeling language Sys ML," in *2017 International Conference on Green Energy Conversion Systems (GECS)*, Hammamet, Tunisia, 2017.

[37] H. R. Galiveeti, A. K. Goswami, and N. B. Choudhury, "Impact of plug-in electric vehicles and distributed generation on reliability of distribution systems," *Engineering Science and Technology, an International Journal*, vol. 21, no. 1, pp. 50–59, 2018.

[38] H. Shokouhandeh and M. Jazaeri, "Robust design of fuzzy-based power system stabiliser considering uncertainties of loading conditions and transmission line parameters," *IET Generation, Transmission & Distribution*, vol. 13, no. 19, pp. 4287–4300, 2019.

[39] H. Shokouhandeh, M. Ghaharpour, H. G. Lamouki, Y. R. Pashakolaei, F. Rahmani, and M. H. Imani, "Optimal estimation of capacity and location of wind, solar and fuel cell sources in distribution systems considering load changes by lightning search algorithm," in *2020 IEEE Texas Power and Energy Conference (TPEC)*, College Station, TX, USA, 2020.

[40] H. Shareef, A. H. Mutlag, and M. Azah, "A novel approach for fuzzy logic PV inverter controller optimization using lightning search algorithm," *Neurocomputing*, vol. 168, no. 1, pp. 435–453, 2015.

[41] L. Luo, W. Gu, Y. Wang, and C. Chen, "An affine arithmetic-based power flow algorithm considering the regional control of unscheduled power fluctuation," *Energies*, vol. 10, no. 11, p. 1794, 2017.

[42] T. Sattarpour, M. Sheikhi, S. Golshannavaz, and D. Nazarpour, "Probabilistic placement of wind turbines in distribution networks," *Electrica*, vol. 18, no. 2, pp. 234–241, 2018.

[43] A. P. Mello, M. Sperandio, D. P. Bernardon et al., "Intelligent system for automatic reconfiguration of distribution network with distributed generation," in *2015 IEEE 5th International Conference on Power Engineering, Energy and Electrical Drives (POWERENG)*, pp. 383–388, Riga, Latvia, 2015.

[44] J. H. Angelim and C. M. Affonso, "Effects of long-range electric vehicles on distribution system using probabilistic analysis," *International Journal of Electrical Power & Energy Systems*, vol. 147, article 108868, 2023.

[45] S. Guner and A. Ozdemir, "Reliability improvement of distribution system considering EV parking lots," *Electric Power Systems Research*, vol. 185, article 106353, 2020.

[46] R. Akbari, R. Hedayatzadeh, K. Ziarati, and B. Hassanizadeh, "A multi-objective artificial bee colony algorithm," *Swarm and Evolutionary Computation*, vol. 2, pp. 39–52, 2012.

[47] L. Ren, Z. Song, C. Mao, and F. Liu, "Multitime scale coordinated scheduling for electric vehicles considering photovoltaic/wind/battery generation in microgrid," *International Transactions on Electrical Energy Systems*, vol. 29, no. 5, article e2821, 2019.